© 2018. Published by The Company of Biologists Ltd | Journal of Cell Science (2018) 131, jcs212886. doi:10.1242/jcs.212886

TOOLS AND RESOURCES

Micropatterning as a tool to identify regulatory triggers and kinetics of actin-mediated endothelial mechanosensing

Florian A. Gegenfurtner[1], Berenice Jahn[1], Helga Wagner[2], Christoph Ziegenhain[3], Wolfgang Enard[3], Ludwig Geistlinger[4], Joachim O. Rädler[5], Angelika M. Vollmar[1] and Stefan Zahler[1,*]

ABSTRACT

Developmental processes, such as angiogenesis, are associated with a constant remodeling of the actin cytoskeleton in response to different mechanical stimuli. The mechanosensitive transcription factors MRTF-A (MKL1) and YAP (also known as YAP1) are important mediators of this challenging adaptation process. However, it is as yet unknown whether both pathways respond in an identical or in a divergent manner to a given microenvironmental guidance cue. Here, we use a micropatterning approach to dissect single aspects of cellular behavior in a spatiotemporally controllable setting. Using the exemplary process of angiogenesis, we show that cell–cell contacts and adhesive surface area are shared regulatory parameters of MRTF and YAP on rigid 2D surfaces. By analyzing MRTF and YAP under laminar flow conditions and during cell migration on dumbbell-shaped microstructures, we demonstrate that they exhibit different translocation kinetics. In conclusion, our work promotes the application of micropatterning techniques as a cell biological tool to study mechanosensitive signaling in the context of angiogenesis.

KEY WORDS: Micropatterning, Mechanosensing, MRTF, MLK1, YAP, Endothelial cell

INTRODUCTION

Morphogenetic processes and the remodeling of existing tissue require the spatiotemporal integration of extracellular mechanical information alongside biochemical guidance cues. The translation of mechanical information into an adapted transcriptional profile is mediated by different routes, including via integrin transmembrane receptors or mechanosensitive ion channels (Isermann and Lammerding, 2013; Mendez and Janmey, 2012). In close interaction with the aforementioned processes, the actin cytoskeleton has a key role in mechanotransduction. The cytoplasmatic actin network is coupled to the nuclear compartment via the LINC protein complex, thus providing a direct transmission route for extracellular mechanical stimuli (Mammoto et al., 2012; Simon and Wilson, 2011). Moreover, a disturbance in the equilibrium between monomeric G- and polymerized F-actin directly influences the subcellular localization of mechanosensitive transcription factors. This mechanism has been described in detail for the growth-controlling serum response factor (SRF) pathway, where the co-transcriptional activator myocardin-related transcription factor (MRTF, which has two isoforms MRTF-A and MRTF-B, also known as MKL1 and MKL2, respectively) is sequestered in the cytoplasm by G-actin (Miralles et al., 2003; Posern and Treisman, 2006). Upon formation of F-actin, this binding is released, thereby enabling nuclear import of MRTF and activation of target gene expression.

A similar, although less directly mediated, effect of actin polymerization on mechanosensitive transcription has been reported for Yes-associated protein (YAP, also known as YAP1), a classic regulator of cell proliferation and the main effector of an evolutionary conserved kinase cascade termed the Hippo pathway (Dupont et al., 2011; Yu and Guan, 2013). MRTF and YAP regulate a variety of shared target genes that are related to cell growth, tissue development and apoptosis (Pan, 2010; Zhao et al., 2010; Chai and Tarnawski, 2002; Mokalled et al., 2015). Connected to this similar physiological role and to their shared activation by actin polymerization (Gaspar and Tapon, 2014; Yu and Guan, 2013), recent work by Yu et al. has provided evidence for a potential crosstalk between MRTF and YAP (Yu et al., 2015).

The sprouting of blood vessels from an existing vascular network is a complex morphogenetic event demanding the orchestration of cellular motility, morphological adaptation and cell division (Potente et al., 2011). The regulatory impact of actin-controlled transcription factors on angiogenesis has received growing attention over the past few years. Franco et al. have shown that SRF is essential for sprouting angiogenesis and the maintenance of vascular integrity (Franco et al., 2008, 2013). Other groups have demonstrated that the MRTF–SRF axis controls blood vessel growth via an adapted expression of CCN1, and that an endothelial-specific ablation of SRF causes vascular disease phenotypes in mice (Hinkel et al., 2014). Concerning the role of Hippo signaling in angiogenesis, YAP has been identified as a key regulator of the angiogenic activators MFAP5 (Marti et al., 2015) and angiopoetin-2 (Choi et al., 2015).

Collectively, the above findings imply that YAP and MRTF have a significant contribution to the regulation of blood vessel formation. However, there is only incomplete knowledge regarding the physiological regulation and activity patterns of these transcription factors in endothelial cells. Most important, the abundance of shared MRTF and YAP target genes gives rise to the question of whether their regulation during vascular development is tightly correlated or if they act in a partially redundant manner. Addressing these questions will contribute to an improved understanding of the recently suggested functional relation between SRF and Hippo signaling (Kim et al., 2016; Speight et al., 2016), not only in angiogenesis, but also in cancer development and its progression in general.

[1]Ludwig-Maximilians-University Munich, Department of Pharmacy, Center for Drug Research, 81377 Munich, Germany. [2]ibidi GmbH, Am Klopferspitz 19, 82152 Martinsried, Germany. [3]Ludwig-Maximilians-University Munich, Department of Biology II, Anthropology and Human Genomics, 82152 Martinsried, Germany. [4]Ludwig-Maximilians-University Munich, Institute for Informatics, Teaching and Research Unit Bioinformatics, 80333 Munich, Germany. [5]Ludwig-Maximilians-University Munich, Faculty of Physics, Soft Condensed Matter Group, 80539 Munich, Germany.

*Author for correspondence (stefan.zahler@cup.uni-muenchen.de)

F.A.G., 0000-0003-2845-9449; H.W., 0000-0002-7003-9512; C.Z., 0000-0003-2208-4877; W.E., 0000-0002-4056-0550; L.G., 0000-0002-2495-5464; A.M.V., 0000-0001-6096-7262; S.Z., 0000-0002-5140-7287

Received 3 November 2017; Accepted 25 April 2018

Journal of Cell Science (2018) 131, jcs212886. doi:10.1242/jcs.212886

In this study, we use a micropatterning approach to characterize the response of MRTF and YAP to spatiotemporally controlled alterations of the cellular microenvironment. We identify the cellular adhesive surface and the number of cell–cell contacts as main regulatory factors of both transcription factors in primary endothelial cells. The use of directly comparative experimental setups enables us to show that MRTF and YAP exhibit differences in the kinetics and sensitivity of their nuclear translocation, which is linked to a different expression of MRTF and YAP target genes at early and late time points in spreading endothelial cells. Our findings are further supported by spatiotemporally distinct MRTF and YAP expression levels and subcellular localization in two angiogenic model systems. Taken together, our data promote the application of micropatterning techniques as a promising *in vitro* tool for studying mechanosensitive aspects of morphogenetic processes. We furthermore provide evidence that, regardless of their shared regulatory triggers, MRTF and YAP might exert distinct functions during angiogenesis, which are based on their respective regulatory kinetics and sensitivity.

RESULTS

Design of micropatterns to mimic mechanosensitive signaling inputs

During the formation of vascular sprouts, many features of endothelial cells change simultaneously: cell–cell contacts, adhesive surface and cell shape. In order to selectively recapitulate microenvironmental aspects of angiogenesis within a highly defined experimental setup, we designed a set of micropatterns derived from a 2500 µm^2-sized square domain as a common starting point, a dimension that is normally occupied by unconfined spreading endothelial cells (Fig. 1). To ensure that the resulting patterns cover a size range that is capable of imposing distinct mechanical challenges on our cells, we analyzed the impact of pattern geometry on the cellular F-actin:G-actin ratio via co-staining of both fractions with phalloidin and DNaseI (Cramer et al., 2002; Nobusue et al., 2014). We found that, when normalized to our reference square, the F-actin:G-actin ratio varied between 80 and 120 within the designed set of micropatterns (Fig. S1).

Endothelial cell–cell junctions inhibit nuclear translocation of MRTF-A and YAP

To analyze the impact of cell–cell contact formation on MRTF-A and YAP subcellular localization, we cultured single endothelial cells on a 2500 µm^2 fibronectin-coated square and compared nuclear levels of MRTF-A and YAP to those on a four-fold larger 10,000 µm^2 pattern harboring four cells under similar confinement and adhesive conditions (Fig. 2A). Quantitative analysis of ≥30 cells for each of the microdomains revealed that upon formation of cell–cell contacts, nuclear levels of MRTF-A and YAP were significantly reduced compared to what was seen on the single-cell setting (Fig. 2B). Of note, the application of microdomains per se led to reduced nuclear levels of both transcription factors (compared to unconfined single cells in Fig. S2), indicating a role of spatial confinement in the regulation of mechanosensitive transcription.

To further assess the specific impact of endothelial cell–cell contacts on the subcellular localization of MRTF-A and YAP, we analyzed the relevance of VE-cadherin-based adherens junctions for this process. After disruption of VE-cadherin (also known as CDH5) junctions within confluent monolayers by means of EGTA, Ca^{2+} levels were restored, and cells were subsequently cultured in the presence or absence of a blocking antibody targeting the extracellular domain of VE-cadherin (Corada et al., 2001) (Fig. 2C). A quantification of the MRTF-A and YAP nuclear intensity per field of view showed that, after an initial translocation due to the readdition of Ca^{2+}, the number of cells showing a predominantly nuclear localization of either of the transcription factors was enhanced in the VE-cadherin-blocked setting compared to the control cells cultured without antibody (Fig. 2D). Our findings were further confirmed by repeating the experiment depicted in Fig. 2A in presence of the anti-VE-cadherin blocking antibody (Fig. S3).

The adhesive surface area and projected nuclear area positively correlates with nuclear levels of MRTF-A and YAP

A common feature of MRTF-A and YAP regulation is the pronounced influence of cell density on the subcellular distribution pattern of these transcription factors. This has previously been reported for various cell lines (Zhao et al., 2007; Mateus et al., 2015; O'Connor et al., 2016), and could be reproduced with primary endothelial cells under standard cell culture conditions in our laboratory (Fig. S2).

However, confluent endothelial cells differ from cells plated at low density in a variety of additional parameters, such as the available adhesive surface area and spatial confinement (Eliceiri and Cheresh, 2001). To examine the influence of these parameters on MRTF-A and YAP subcellular localization, we quantified the nuclear levels of both transcription factors for cells cultured on a set of square microdomains featuring a stepwise increase in total surface area ranging from 30 to 60 µm edge length (Fig. 3A). A

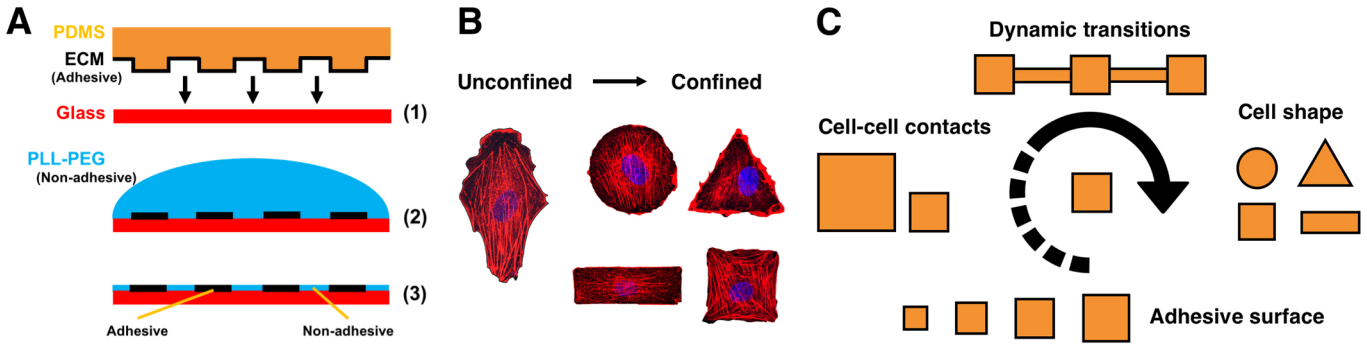

Fig. 1. Application of micropatterns to study the influence of extracellular physical cues on endothelial mechanosensing. (A) Microcontact printing (µCP) was used for the generation of fibronectin-coated microdomains surrounded by a non-adhesive poly-L-lysine–polyethylene glycol (PLL-PEG) layer, allowing for *in vitro* culture and analysis of a single HUVEC under highly controlled microenvironmental conditions. (B) Representative images of single endothelial cells grown under unconfined conditions (left) and on differently shaped microdomains (right). (C) Based on a 50×50 µm square as common starting point, four different sets of microfeatures were generated to study the regulation of MRTF-A and YAP in endothelial cells.

Journal of Cell Science (2018) 131, jcs212886. doi:10.1242/jcs.212886

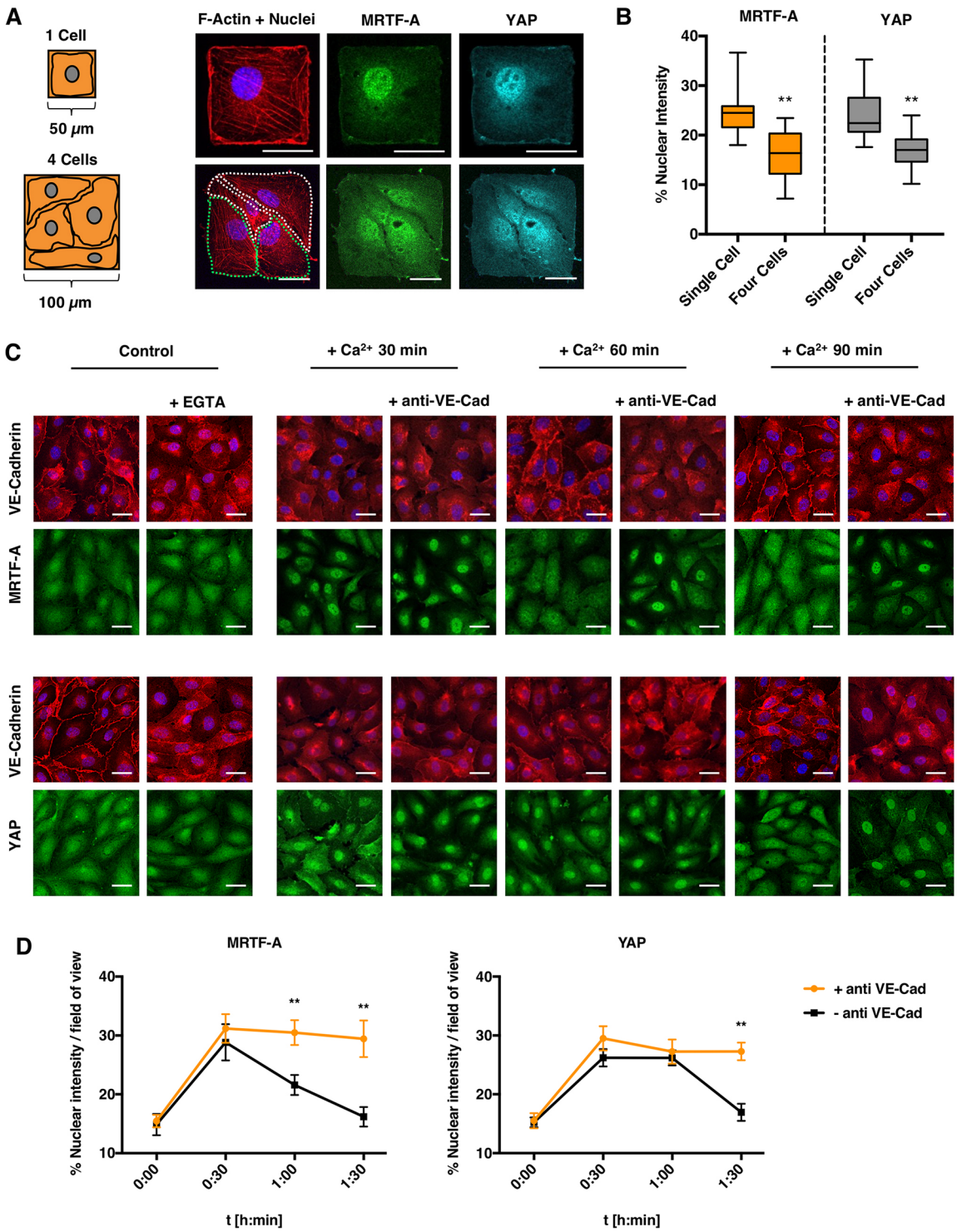

Fig. 2. Loss of cell–cell contacts triggers nuclear translocation of MRTF-A and YAP in HUVECs. (A) HUVECs were seeded onto the illustrated patterns and, after 20 h, co-stained for F-actin, MRTF-A and YAP. Scale bars: 35 µm. (B) Nuclear levels of MRTF-A and YAP in terms of nuclear intensity/total intensity were quantified in ≥30 cells for each of the two patterns in three independent experiments. On the 10,000 µm^2 pattern, only cells with an area of 2500 µm^2±200 µm^2 and an aspect ratio between 1:1 and 1:1.5 were analyzed (marked by green lines in A). Data is presented as a box-and-whisker plot. The box represents the 25–75th percentiles, and the median is indicated. The whiskers show the range. $^{**}P$<0.01 (Student's *t*-test). (C) Confluent HUVECs were pre-treated with EGTA to disrupt VE-cadherin-containing cell junctions (left panel). After re-addition of Ca^{2+}, cells were incubated with (+anti VE-Cad) or without an antibody blocking the extracellular domain of VE-cadherin and subsequently stained for MRTF-A (top) or YAP (bottom). Scale bars: 10 µm. (D) Nuclear intensities of MRTF-A and YAP per field of view were quantified in at least five regions per setting (≥50 cells) after 30, 60 and 90 min. $^{**}P$<0.01 (Sidak-corrected one-way ANOVA test).

quantification of nuclear MRTF-A levels gave a strong correlation to the size of the provided adhesive surface when intensity was normalized to the respective compartment area within the tested range of patterns (Fig. 3B). We observed the same effect – although less pronounced – for nuclear levels of YAP (Fig. 3B). As well as a correlation between MRTF-A and YAP nuclear levels and the

Journal of Cell Science (2018) 131, jcs212886. doi:10.1242/jcs.212886

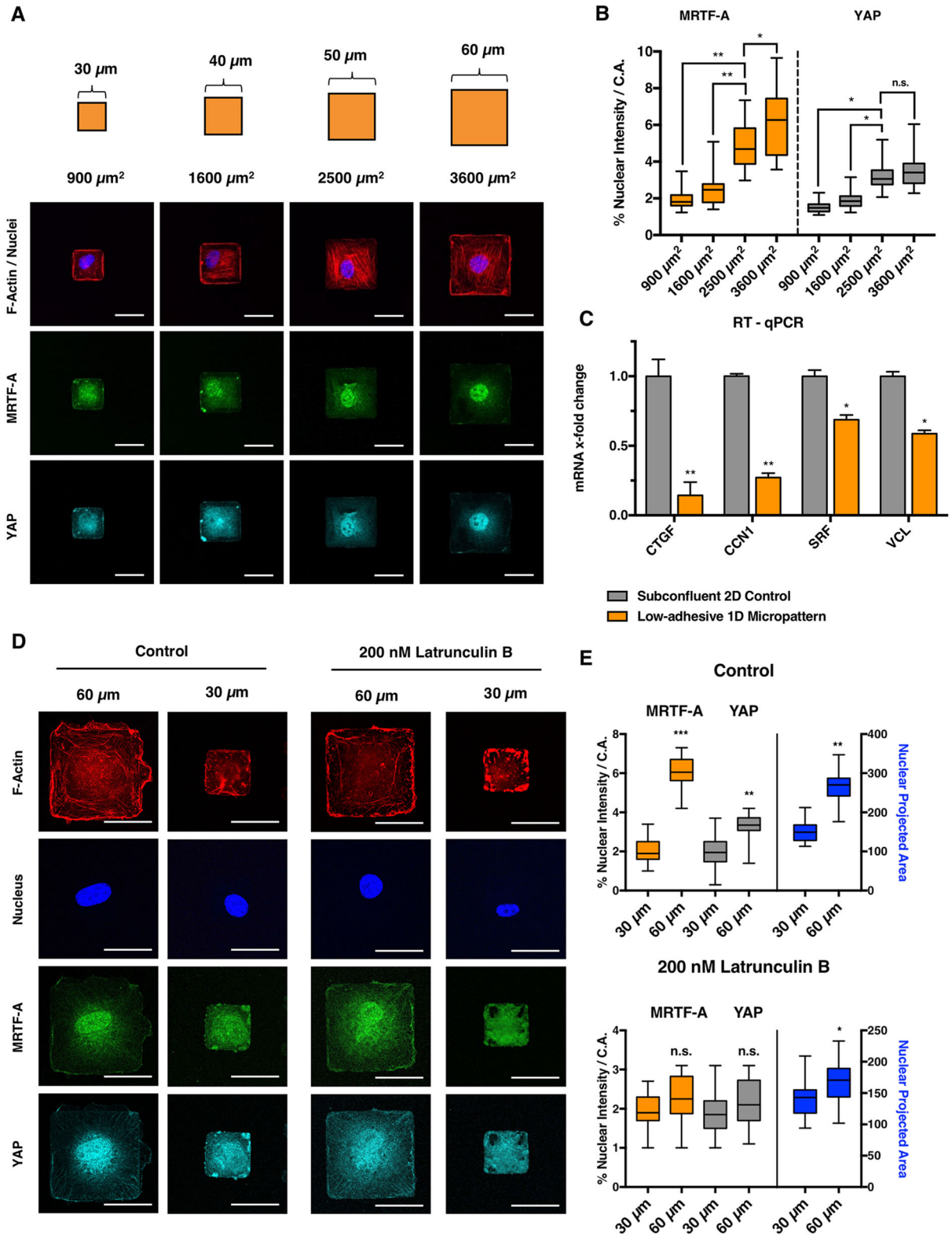

Fig. 3. Adhesive surface and nuclear projected area correlate with nuclear levels of MRTF-A and YAP. (A) Single HUVECs were seeded onto square micropatterns of varying surface areas ranging from 900 to 3600 μm^2. After 20 h, cells were stained for F-actin, MRTF-A and YAP. (B) Nuclear levels of both transcription factors in terms of nuclear intensity/total intensity were quantified in ≥30 cells derived from three independent experiments and normalized to the respective compartment area. *P<0.05; **P<0.01; n.s., not significant (Sidak-corrected one-way ANOVA test). (C) mRNA expression levels of prominent SRF and Hippo target genes were analyzed in HUVEC lysates collected from cells grown under normal 2D cell culture conditions and compared to that of cells grown on low-adhesive linear microtracks (3 μm line width). Relative mRNA levels (mean±s.d.) are normalized to GAPDH. *P<0.05, **P<0.01 (unpaired Student's t-test). (D,E) Nuclear projected area was analyzed on the 900 and 3600 μm^2 squares described in A. Cells were left untreated or stimulated with 200 nM latrunculin B. Data is derived from ≥30 cells in three independent experiments. P<0.05; **P<0.01; **P<0.001; n.s., not significant (Student's t-test). Data in B and E are presented as box-and-whisker plots. The box represents the 25–75th percentiles, and the median is indicated. The whiskers show the range. Scale bars: 30 μm.

Journal of Cell Science (2018) 131, jcs212886. doi:10.1242/jcs.212886

provided adhesive area, we also observed an increase in the nuclear projected area on larger patterns. The increase in nuclear projected area, a previously described indicator of intracellular mechanical tension (Buxboim et al., 2017), could be rescued by stimulation with the actin-depolymerizing compound latrunculin B (Fig. 3D,E). In addition, stimulation with latrunculin B also impaired nuclear translocation of MRTF-A and YAP on the 3600 μm^2 square.

To determine whether the redistribution of MRTF-A and YAP to the nuclear compartment in response to an increased adhesive surface area caused an increase in transcription of target genes, we performed real-time quantitative PCR (RT-qPCR) experiments on shared target genes of the MRTF–SRF and the Hippo–YAP signaling axes. For this purpose, we compared mRNA levels of sparsely cultured human umbilical vein endothelial cells (HUVECs) with infinite spreading area to the expression levels of cells cultured on low-adhesive narrow microtracks, which have been previously described in detail in our laboratory (Schuster et al., 2016). Compared to the square patterns described in Fig. 3A, which are sometimes occupied by multiple cells, the linear microtracks offer the advantage to collect lysates from a cell population that homogeneously has a low adhesive area. In good agreement with our immunofluorescence data on the subcellular localization of MRTF-A and YAP, the expression levels of all tested target genes were significantly downregulated for cells in the setting with a small adhesive area when compared to the cells cultured on an unconfined planar surface (Fig. 3C).

Endothelial cell shape has a minor impact on MRTF-A and YAP nuclear levels

Following the analysis of cell–cell contacts and adhesive surface area, we next examined how a predefined shape of the cell might affect the regulation of mechanosensitive transcription factors MRTF-A and YAP. For this, we seeded endothelial cells on 2500 μm^2 patterns of different geometries (Fig. 4A) and quantified the nuclear levels of MRTF-A and YAP after 20 h in the same way as for the experiments described above. We found that, unlike the provided adhesive surface area or the number of cell–cell contacts, an alteration of cell shape had no significant effect on the subcellular localization of either of the transcription factors (Fig. 4B). Remarkably, although the morphology and, in particular, the orientation of stress fibers was clearly influenced by pattern geometry, we did not see a connection to the subcellular localization of MRTF-A and YAP in our experiments.

MRTF-A and YAP exhibit differential regulatory kinetics in endothelial cells

Having shown that MRTF-A and YAP react similarly to a variation of microenvironmental properties under static conditions, we next aimed to analyze the regulatory kinetics of both transcription factors in a dynamic, yet spatiotemporally controlled, experimental setup. For this purpose, we designed a micropattern composed of interconnected squares (a dumbbell shape), which forces cells to adapt their morphology in a manner resembling the sprouting of endothelial tip cells (Fig. 5A). To study subcellular localization of

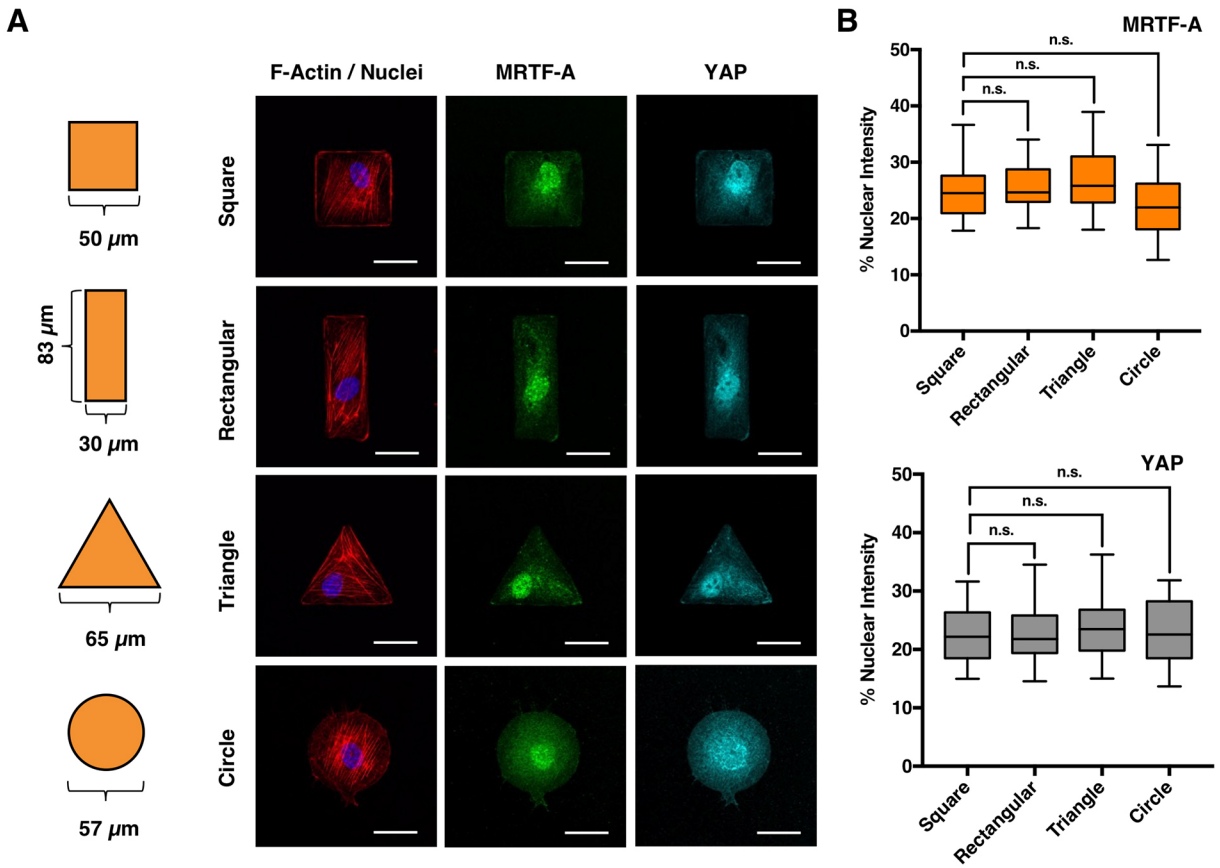

Fig. 4. Static variation of cell shape has a minor impact on MRTF-A and YAP subcellular localization in HUVEC. (A) Single HUVECs were seeded onto 2500 μm^2 micropatterns of different geometries. After 20 h, cells were co-stained for F-actin, MRTF-A and YAP. Scale bars: 30 μm. (B) Nuclear levels of both transcription factors in terms of nuclear intensity/total intensity were quantified in ≥30 cells in at least three independent experiments. Data is presented as a box-and-whisker plot. The box represents the 25–75th percentiles, and the median is indicated. The whiskers show the range. n.s., not significant (Sidak-corrected one-way ANOVA test, P>0.05).

Journal of Cell Science (2018) 131, jcs212886. doi:10.1242/jcs.212886

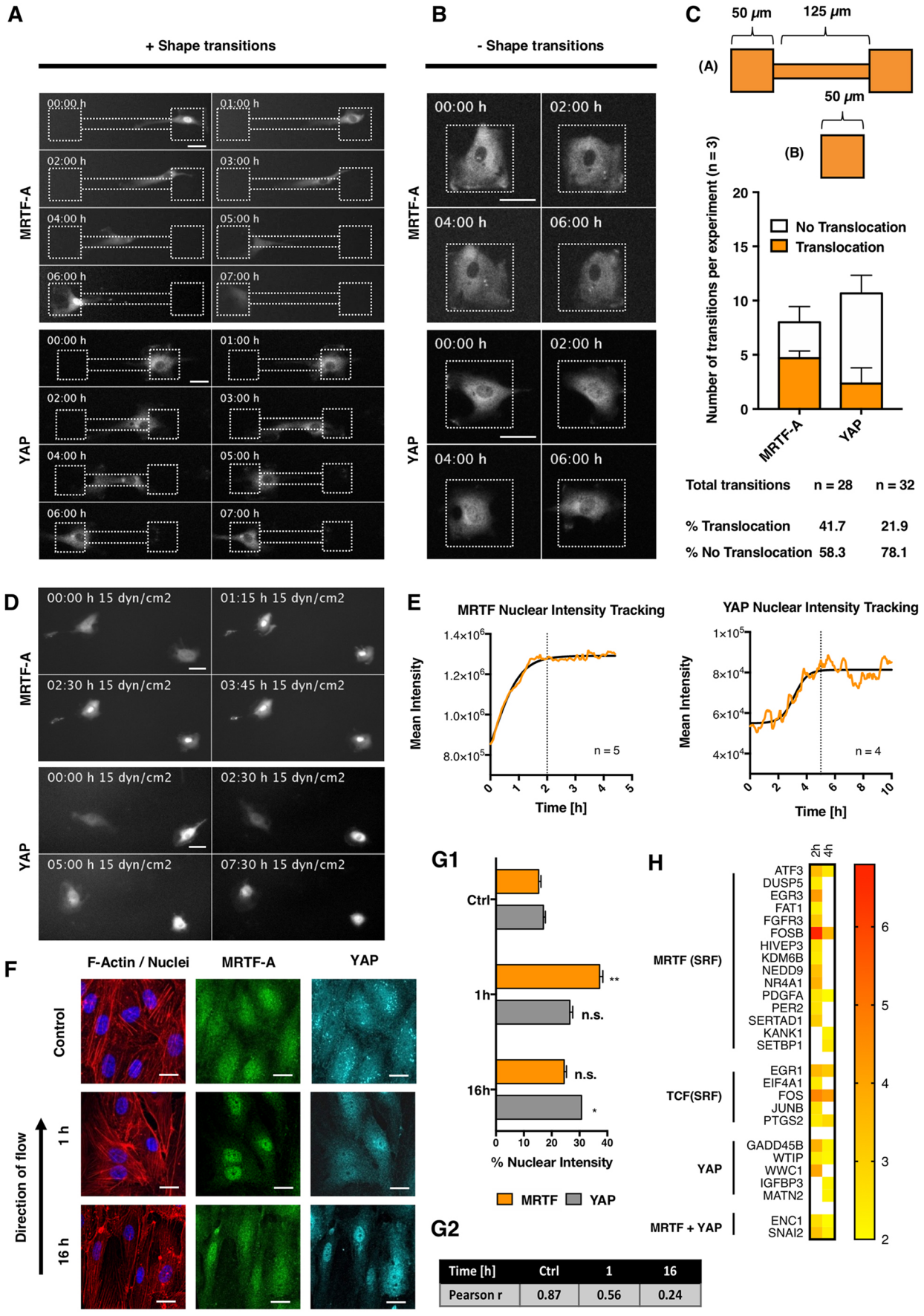

Fig. 5. See next page for legend.

Journal of Cell Science (2018) 131, jcs212886. doi:10.1242/jcs.212886

Fig. 5. MRTF-A and YAP exhibit differential regulatory kinetics in endothelial cells. (A,B) Subconfluent HUVECs were transiently transfected with MRTF-A–GFP or hYAP1–GFP expression vectors and, after 24 h, seeded either onto a micropattern composed of interconnected squares (A) or onto unconnected control patterns (B). Cell migration was subsequently analyzed by time-lapse imaging over the indicated time spans. Scale bars: 30 µm. (C) Top, pattern geometries of the experiments in A and B. Bottom, quantification of MRTF-A and YAP translocation events. Relative numbers are normalized to the total number of shape transitions. Results are mean±s.d. (D) MRTF-A–GFP- or hYAP1–GFP-expressing HUVECs were subjected to laminar shear stress (15 dyn/cm^2) and analyzed by time-lapse imaging in flow chambers for indicated time spans. (E) Mean time traces for nuclear intensities of MRTF and YAP in representative cells from two independent experiments. (F,G) Representative immunofluorescence staining images and nuclear intensity quantification (mean±s.d.) of endogenous MRTF-A and YAP after 1 and 16 h of cultivation under the flow conditions described in D. *P<0.05; **P<0.01; n.s., not significant (Sidak-corrected one-way ANOVA). Pearson coefficients (r above threshold) were calculated to express the correlation between YAP and MRTF-A intensity distribution at indicated time points. Scale bars: 30 µm. (H) Transcriptome heatmap showing upregulated ($\log_2$ fold change >2) MRTF-, TCF- and YAP-driven target genes in spreading endothelial cells; analyzed data refers to confluent control cells. A full list of all upregulated genes is available as Table S1.

MRTF-A and YAP in live cells, we used MRTF-A–GFP and hYAP1–EGFP plasmid constructs. Although their subcellular distribution is different from the endogenous proteins in resting cells (Fig. 2A), the GFP-tagged variants can be used to study the kinetics of translocation in migrating or mechanically stressed cells. Fluorescence time-lapse imaging of MRTF-A–GFP- and hYAP1–EGFP-expressing HUVECs revealed that, during migration across the pattern, MRTF-A frequently translocated between the nuclear and the cytoplasmatic compartment in response to the morphological challenge imposed by the transition between adjacent squares (Fig. 5A, top panel, Fig. 5C). In detail, reaching a square after a migratory interphase served as a trigger for translocation of MRTF-A. However, we observed a significantly smaller rate of redistribution events for YAP, which remained mostly cytoplasmatic in our experiments (Fig. 5A, bottom panel, Fig. 5). Of note, neither MRTF-A nor YAP exhibited nuclear redistribution when imaged on unconnected control squares, thus confirming that the translocation of MRTF-A was no random event but indeed triggered by the morphological transitions provoked by our pattern (Fig. 5B).

Apart from the morphological challenges imposed on cells during the migration in angiogenesis and wound healing, shear stress is among the most important extracellular forces encountered by the endothelium (Chatterjee et al., 2015). To verify our hypothesis that MRTF is more sensitive and/or relocalizes faster to a given mechanical stimulus than YAP, the subcellular localization of both transcription factors was analyzed under laminar flow conditions (Fig. 5D). We therefore subjected MRTF-A–GFP- and hYAP1–EGFP-expressing HUVECs to a constant shear stress of 15 dyn/cm^2 and recorded the nuclear intensity traces for both transcription factors over time (Fig. 5E). Consistent with our findings on migrating cells, we observed that MRTF-A rapidly responded to shear stress by translocating to the nucleus within minutes. In contrast, maximal nuclear accumulation of YAP was delayed by several hours, which could be confirmed by endpoint measurements of endogenous MRTF-A and YAP in fixed and immunostained cells (Fig. 5F,G).

As a final point, we addressed the question of whether the above-described differential regulatory kinetics could be linked to time-dependent variations of MRTF-A and YAP target gene expression. We therefore generated transcriptome data (RNA-seq) of spreading endothelial cells at early (2 h) and late (4 h) time points after plating and compared the number of upregulated ($\log_2$ fold change >2) MRTF and YAP target genes based on recently published lists for the CArG box (Esnault et al., 2014) and TEAD (Zanconato et al., 2015) promoters (Fig. 5H). We found that, in support of our live-cell imaging data, the number of upregulated MRTF-dependent SRF target genes was strongly reduced after 4 h, whereas YAP and shared YAP/MRTF target genes showed a more consistent expression over time.

Expression and nuclear redistribution of MRTF-A is spatiotemporally distinct from YAP in angiogenic model systems

To confirm our experimental data on the regulatory parameters and kinetics of MRTF-A and YAP nuclear translocation in a setting resembling the *in vivo* situation, we analyzed subcellular localization and expression of both transcription factors in two frequently used angiogenic model systems. For endothelial tube formation experiments, 200,000 cells/ml were seeded on top of thin Matrigel™ layers and, after 6 and 20 h, co-stained for MRTF-A and YAP (Fig. 6A). The correlation of expression levels at different positions within the nascent network (marked by white boxes) was assessed by calculating the Pearson's correlation coefficient above threshold (Fig. 6C). Additionally, the subcellular localization of MRTF-A and YAP was determined via intensity quantification in Hoechst-positive areas in relation to the total signal intensity (Fig. 6B).

The representative images in Fig. 6A indicate high expression levels for MRTF-A at mechanically strained tip regions and in cells located in close proximity to the border of the network. In contrast, both expression levels and nuclear levels of MRTF-A were significantly less pronounced at nodal points and in inner network regions. For YAP, we observed a similar tendency (Fig. 6B). As well as a location-dependent variation of subcellular localization, we also noticed time-dependent differences in the correlation between MRTF-A and YAP, presumably owing to a slower increase of nuclear YAP levels (maximal nuclear accumulation after 20 h). Connected to this, the intensity distribution of MRTF-A and YAP was better correlated at the late time point (0.77 after 20 h) compared to the earlier one (0.29 after 6 h), which is in good agreement with the temporal differences in MRTF-A and YAP nuclear translocation observed in our perfusion assay experiments (Fig. 5). Of note, nuclear levels of MRTF-A and YAP on Matrigel™ were generally lower than under standard cell culture conditions (Fig. S2). This was presumably due to the varying stiffness of both materials (Dupont et al., 2011), which was supported by a stiffness-dependent subcellular localization of MRTF-A and YAP on polydimethylsiloxane (PDMS) surfaces (Fig. S4). Based on the above findings, we developed a model illustrating the basic regulatory triggers and translocation dynamics of MRTF-A and YAP in endothelial cells *in vitro* (Fig. 6D).

To examine the tissue-specific expression of MRTF and YAP in *in vivo*, we analyzed the expression patterns of MRTF-A and YAP in the developing retinal vasculature of postnatal day 6 (P6) C57BL/6 mice.

As shown in the upper panels of Fig. 6E, MRTF-A is highly expressed in tip and stalk cells of vascular sprouts, which is in line with previous reports for the MRTF–SRF pathway by Franco et al. (Franco et al., 2013). Remarkably, we observed an inverse expression pattern for YAP, which was predominantly expressed in perfused vessels of the mature inner retinal vasculature (Fig. 6E, bottom panel).

Journal of Cell Science (2018) 131, jcs212886. doi:10.1242/jcs.212886

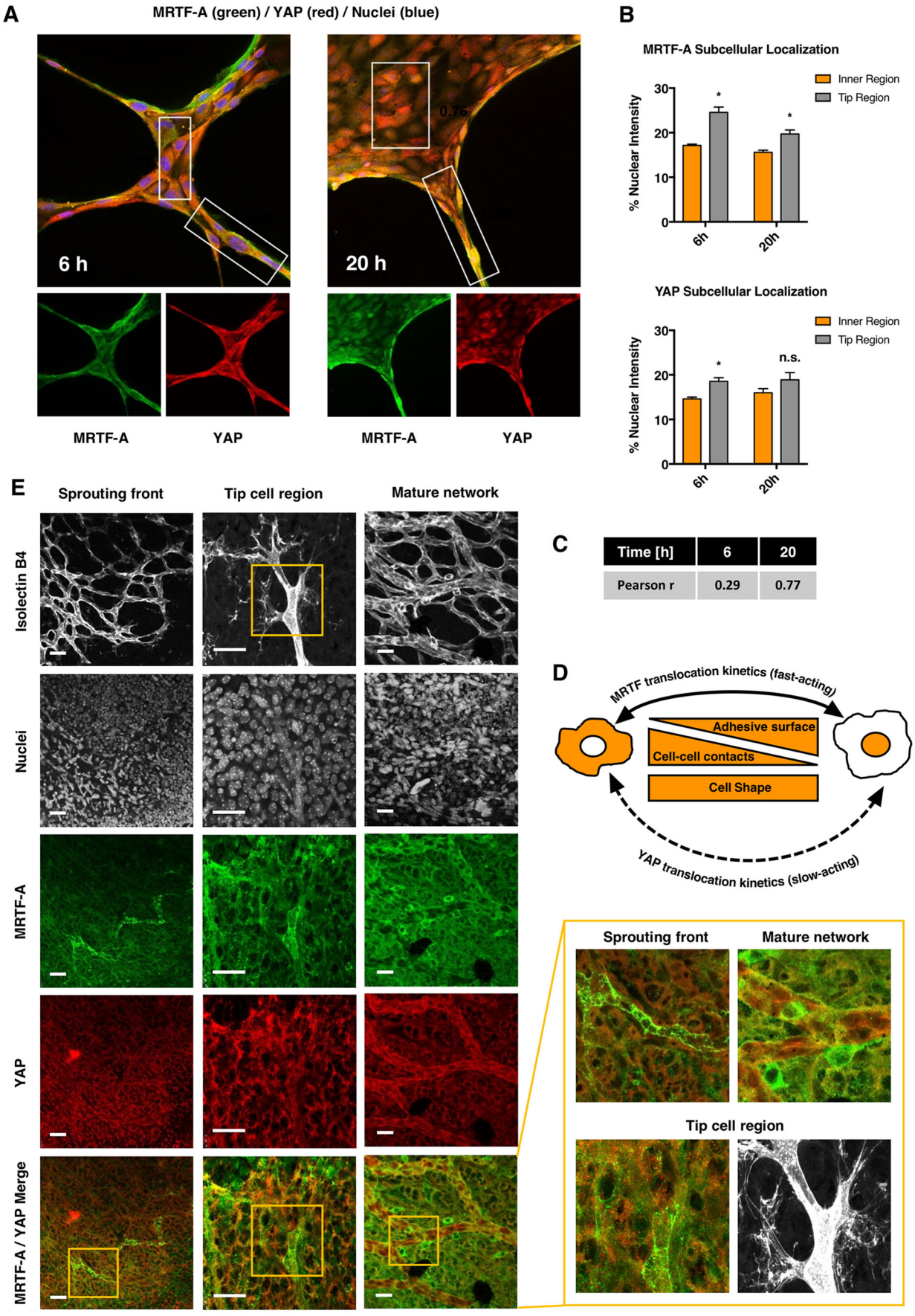

Fig. 6. See next page for legend.

Journal of Cell Science (2018) 131, jcs212886. doi:10.1242/jcs.212886

Fig. 6. Nuclear redistribution of MRTF-A is spatiotemporally distinct from that of YAP in angiogenic model systems. (A) Endothelial cells (11×10^3) were seeded onto thin layers of Matrigel™ and incubated for the indicated time spans. Tubular structures were co-stained for F-actin, the nucleus, MRTF-A and YAP. A region was regarded as 'inner' if it made at least three contacts with neighboring cells. Representative examples for each of the two regions are highlighted by white boxes. (B) Subcellular localization of MRTF-A and YAP was determined via intensity quantification in Hoechst 33342-positive areas in relation to the total signal intensity. Results are mean±s.e.m. from four independent experiments. Three regions were analyzed in each experiment. *P<0.05 (multiple t-tests using the Bonferroni-Dunn method). (C) Pearson coefficients (r above threshold) were calculated to express the correlation between YAP and MRTF-A intensity distribution at early (6 h) and late (20 h) time points. (D) Proposed model showing regulatory triggers and kinetic properties of MRTF-A and YAP in endothelial cells. (E) Wild-type C57BL/6 retinal whole-mounts (n=8) were prepared at P6. Retinal vasculature is visualized by Isolectin B4 labeling and samples are co-stained for MRTF-A and YAP. Representative images for the sprouting front and the inner network are shown. Scale bars: 30 µm.

Taken together, our results show that subcellular localization of MRTF-A and YAP is regulated in a time- and location-dependent manner during tubular network formation *in vitro*. In addition to this, we observed differential expression patterns in the developing retinal vasculature *in vivo*.

DISCUSSION

The sprouting of blood vessels from an existing vascular network involves the spatiotemporally coordinated degradation of and, thereafter invasion into, the surrounding extracellular matrix. This requires a careful sensing and then adaptation of the cell to changing biophysical properties (Chatterjee et al., 2015; Santos-Oliveira et al., 2015). Over the past years, the vast majority of work on endothelial mechanosensing has focused on vascular remodeling processes and altered redox signaling in response to fluid shear stress (Ando and Yamamoto, 2009; Chatterjee et al., 2015; Tzima et al., 2005). However, current knowledge on the physiological role and on the regulatory behavior of mechanosensitive signaling pathways in the context of angiogenesis is limited. To date, it is only known that MRTF and YAP are both mandatory for vascular development. However, the question of whether these two mechanoresponsive signaling pathways are redundant backup systems or whether they, at least partially, collaborate (Yu et al., 2015; Kim et al., 2016) remained open.

By varying the cell number on differently sized micro-adhesive squares, we observed that the loss of endothelial cell–cell contacts, a hallmark event in angiogenesis, serves as a trigger for nuclear translocation of both MRTF-A and YAP (Fig. 2). The role of cell–cell junctions in general, and of VE-cadherins in particular, in regulating YAP subcellular localization has recently been described by Giampietro et al. (Giampietro et al., 2015). We could confirm part of this work with our VE-cadherin-blocking experiments and furthermore observed a functionally similar, although kinetically different, response for MRTF-A. Our work thus expands the regulatory impact of VE-cadherins on endothelial mechanosensing to affecting the MRTF–SRF axis. Of note, the involvement of cadherin family proteins in the regulation of MRTF is presumably not limited to VE-cadherins, since Busche et al. have reported similar findings for epithelial cell cadherins (Busche et al., 2008).

Apart from the above-described sensitivity towards a gain or loss of cell–cell contacts, our studies revealed that the provided total adhesive surface area has a pronounced influence on nuclear levels of both MRTF-A and YAP (Fig. 3). On a transcriptional level, this was confirmed by the clearly reduced expression of MRTF and YAP target genes in a microenvironment with a small adhesive area. In good agreement with our finding that an increase in the adhesive area results in the nuclear accumulation of MRTF-A, recent work by Plessner and colleagues established a connection between integrin signaling, Rho GTPase activation and SRF-mediated transcription via nuclear actin polymerization (Plessner et al., 2015). This is consistent with results from Hermann et al., who demonstrated that integrin signaling synergizes to trigger the expression of the invasion-promoting SRF target gene *ISG15* (Hermann et al., 2016).

In line with our findings for MRTF-A, we also observed a clear correlation between adhesive surface area and nuclear levels of the transcription factor YAP. The mechanism underlying this regulation is incompletely understood. It has been previously shown by Zhao et al. that cell detachment initiates Lats 1/2 kinase activity and, therefore, YAP phosphorylation and its cytoplasmic retention in MCF10A cells (Zhao et al., 2012). An increase in adhesive surface area is known to trigger DNA synthesis, as has been reported decades ago for mouse fibroblasts on differently sized adhesive islands (Ireland et al., 1987; O'Neill et al., 1986). Being a major regulator of cell proliferation, it is likely that YAP activation, through increased adhesive surface, rather than a change in cell shape (Fig. 4), contributes to cell cycle entry. Mechanistically, a direct connection between integrins and Hippo signaling has been suggested (Dupont, 2015). In our experiments, the nuclear levels of MRTF-A and YAP were not only correlated within the global cell population but also on a single-cell level (Fig. S5). It is therefore likely that integrins are a shared regulator of MRTF-A and YAP, as it is the case for VE-cadherins in the context of cell–cell contacts (Fig. 2).

As a third parameter besides adhesive surface and cell–cell contacts, we tested how a variation of cell shape affects the subcellular localization of both transcription factors. Although we saw that nuclear levels of MRTF-A and YAP were reduced in comparison to what was seen in cells in an unconfined control setting (Fig. 4; Fig. S2), we did not observe a shape-dependent regulation within the range of tested micropatterns. Interestingly, O'Connor et al. have reported a shape factor-dependent regulation of the SRF target TGF-β in epithelial cells under similar, although not completely identical, experimental conditions (O'Connor and Gomez, 2013). On the other hand, a global analysis of gene expression patterns performed by Stiles et al. has demonstrated that spatial confinement per se, but not a particular cell shape, is the master regulator of an adapted transcriptional profile in human coronary artery endothelial cells (Stiles et al., 2013). Since our observations in HUVECs point in a similar direction, there might be cell- or at least tissue-specific differences regarding the impact of cell shape on transcriptional regulation. Of note, a direct deformation of the nucleus is known to affect chromatin organization and therefore gene expression in a variety of cell lines (Dechat et al., 2008; Isermann and Lammerding, 2013; Thomas et al., 2002; Versaevel et al., 2014). Therefore, it is important to point out that the different pattern geometries used in our studies influenced cellular but not nuclear shape (Fig. S1).

The similar static response of MRTF-A and YAP to our different micropatterns did not allow us to draw conclusions on potential kinetic variations in their regulation. We therefore analyzed translocation dynamics of both transcription factors during migration across a structurally challenging dumbbell-shaped micropattern (Fig. 5). Our time-lapse imaging experiments on these interconnected micro-squares indicated that MRTF-A is much more sensitive to this stimulus than YAP. Furthermore, the response of YAP to fluid shear stress (Fig. 5) was delayed compared to the rapid nuclear redistribution of MRTF-A. In line with this,

Journal of Cell Science (2018) 131, jcs212886. doi:10.1242/jcs.212886

cytoplasmic relocalization of YAP, for example, after reformation of cell–cell contacts (Fig. 2), was also markedly slower than in the case of MRTF-A. Another intriguing possibility is that the migration across this pattern is associated with distinct modes of cytoskeletal reorganization, as was recently described by Kim et al. (Kim et al., 2014).

The regulation of YAP under shear stress has recently been controversially discussed in terms of an activating (Nakajima et al., 2017) or inactivating (Xu et al., 2016) response to this stimulus. Therefore, it is possible that YAP is only activated in response to distinct mechanical stimuli, as it has been suggested for disturbed flow conditions (Wang et al., 2016). More recently, a solely force-dependent mechanism of nuclear YAP entry and exit has been described (Elosegui-Artola et al., 2017). Interestingly, YAP could be rapidly activated in our cells with thrombin (Fig. S6), which points to the direction that its activation is not generally slow but rather dependent on the respective physiological context.

Our hypothesis on differential regulatory kinetics of MRTF-A and YAP in endothelial cells is supported by immunofluorescence co-stainings of both transcription factors at different stages of tubular network formation. In these experiments, MRTF-A expression levels were already considerably reduced at nodal points of the inner network compared to levels in the dynamic border regions by 2 h after plating (Fig. 6). The reduction of total expression levels was accompanied by a significant drop in nuclear MRTF-A levels within confluent areas. However, we did not observe an equally rapid cytoplasmic redistribution for YAP, which exhibited less pronounced differences in subcellular localization between outer and inner regions. The slow regulation of YAP was further reflected by a more consistent expression over time, resulting in a time-dependent variation of its correlation to MRTF-A expression (Fig. 6).

Our direct comparison of translocation dynamics, expression levels and subcellular localization of MRTF-A and YAP suggests that the kinetics and sensitivity of nuclear translocation are two of the most striking differentiators in the regulation of both transcription factors. In line with our present data for primary endothelial cells, Cui et al. have reported that MRTF-A translocates much faster than YAP when fibroblasts are subjected to cyclic stretching forces (Cui et al., 2015). More recently, a study from the Posern group has highlighted that a precise temporal control of MRTF-A is required for the formation of mammary acini (Seifert and Posern, 2017).

A potential explanation for the divergent regulatory kinetics of MRTF-A and YAP could be found by looking at the differential role of actin in the two associated signaling cascades. In the case of MRTF-A, its subcellular localization is directly coupled to the F-actin to G-actin equilibrium (Posern et al., 2002). On the other hand, YAP is indirectly influenced by actin polymerization – presumably via angiomotins (Mana-Capelli et al., 2014; Chan et al., 2011). Moreover, the canonical Hippo cascade is regulated by a variety of different stimuli (Yu and Guan, 2013), which could at least partially counteract the cytoskeletal influence.

Based on the above findings, we suggest that – regardless of their shared activating stimuli – MRTF-A and YAP serve distinct functions in the transcriptional regulation of endothelial cells. Owing to its above-mentioned direct coupling to the polymerization state of actin, MRTF-A could fulfill the role of a fast-responding mechanosensitive switch that is rapidly activated at nascent sprouts and required for the highly dynamic process of tip cell invasion. In turn, the limited responsiveness of YAP to cytoskeletal remodeling points to the direction that this transcription factor could, once activated, serve to sustain a basal proliferative activity in endothelial cells during vessel development and maturation. On a functional level, this hypothesis is supported by the time-dependent expression of MRTF-A and YAP target genes in our transcriptome approach (Fig. 5) and by the different expression patterns of both transcription factors in the developing murine retina (Fig. 6).

In conclusion, our work provides a systematic comparative analysis of microenvironmental cues for the mechanosensitive regulation of blood vessel formation. Based on the application of micropatterning techniques as a tool to mimic the mechanobiological aspects of angiogenesis, we identify the loss of cell–cell contacts and changes in adhesive surface as major regulators of both MRTF-A and YAP nuclear translocation in endothelial cells. Apart from these similarities, we observe that MRTF-A exhibits significantly higher responsiveness than YAP on a shorter time scale, suggesting that both transcription factors are assigned different tasks in the spatiotemporal regulation of angiogenesis.

MATERIALS AND METHODS

Cell culture

HUVECs were purchased from Promocell (Heidelberg, Germany). Cells were cultivated with ECGM Kit enhanced (PELO Biotech, Planegg, Germany) supplemented with 10% fetal calf serum (FCS; PAA Laboratories GmbH, Pasching, Austria) and 1% penicillin/streptomycin/amphotericin B (all purchased from PAN-Biotech, Aidenbach, Germany). Upon reaching confluency, cells were counted on a ViCell XR device (Beckmann Coulter, Munich, Germany) and split 1:2 and cultured for a maximum of six passages. Cells were cultivated at 37°C under an 5% CO_2 atmosphere. To ensure equal adhesive conditions across different assay formats, fibronectin-coated surfaces were used in all experiments.

Plasmids and transfections

Primary endothelial cells were transiently transfected using the Targefect-HUVEC™ transfection kit (Targeting Systems, El Cajon, CA) according to manufacturer's instructions. Live-cell imaging was performed between 24 and 48 h after transfection.

GFP-tagged murine MRTF-A was a kind gift from the laboratory of Prof. Robert Grosse (Marburg, Germany). pEGFP-C3-hYAP1 was obtained from Addgene (#17843; Basu et al., 2003).

Live-cell imaging and perfusion assays

Live-cell imaging experiments were performed on a Nikon Eclipse Ti Inverted Microscope (Nikon, Düsseldorf, Germany) equipped with a 4×/0.13 NA PlanFluor objective and a Cool LED pE-100 excitation light source. Cells were imaged at 37°C under a 5% CO_2 atmosphere and at 80% humidity using a heating and gas incubation system from ibidi (Martinsried, Germany).

Unidirectional flow culture experiments were performed with an ibidi Pump System. 4×10^5 HUVECs were seeded into fibronectin-coated µ-Slides I 0.4 Luer (ibidi, Martinsried, Germany) 2 days before the experiment and transiently transfected with GFP-labeled MRTF-A or YAP 24 h before imaging. Shear stress was kept constant at 15 dyn/cm^2, resulting in a final flow rate of ∼15 ml/min.

Microcontact printing

Microcontact printing (µCP) was performed as previously described (Schuster et al., 2016). In brief, PDMS stamps were crafted from silicon template wafers carrying the desired microfeatures (Fig. 1). After UV-induced surface hydrophilization, stamps were coated with 50 µg/ml fibronectin (BD, Franklin Lakes, NJ) for 2 h and subsequently washed with sterile H_2O. The protein pattern was then transferred onto the surface of uncoated eight-well µ-Slides from ibidi (Martinsried, Germany) via µCP. Surrounding areas were blocked for cell adhesion using a sterile aqueous solution of 1 mg/ml PLL-[2]-PEG (Surface Solutions, Dübendorf, Switzerland).

Laser scanning confocal microscopy

Confocal images were acquired using a Leica TCS SP8 SMD microscope equipped with the following HC PL APO objectives: 40×/1.30 NA oil, 63×/

1.40 NA oil or 63×/1.20 NA W Corr. Pinhole size was adjusted to 1.0 airy units and scanning was performed at 400 Hz. An average of four frames was acquired for every channel in sequential scanning mode. The following laser lines were used for excitation: 405 nm, 488 nm, 561 nm and 647 nm.

Antibodies, compounds and staining reagents

The following primary antibodies were used for this study were against: MRTF-A (G-8) mouse mAb IgG_{2a}, sc-390324 (Santa Cruz Biotechnology, Dallas, TX); VE-cadherin^{ECD}, mouse mAb IgG_{2a}, MABT134 (Merck Millipore, Darmstadt, Germany); VE-cadherin (D87F2) XP® rabbit mAb (Cell Signaling Technology, Danvers, MA); YAP (B-8) mouse mAb IgG_{2a}, sc-398182 (Santa Cruz Biotechnology); YAP (D8H1X) XP® rabbit mAb (Cell Signaling Technology). The following secondary antibodies were used for this study: Alexa Fluor 488-conjugated goat anti-mouse IgG (H+L), A-11001; Alexa Fluor 647-conjugated goat-anti-rabbit IgG (H+L), A-21245; Alexa Fluor 546-conjugated goat-anti-mouse IgG (H+L), A-11030 (all from ThermoFisher, Waltham, MA).

Latrunculin B was purchased from Sigma. Rhodamine–phalloidin and Hoechst 33342 were purchased from Sigma and used at a dilution of 1:400 (phalloidin) or at a final working concentration of 0.5 µg/ml (Hoechst). FluorSave Reagent mounting medium was purchased from Merck Millipore (Darmstadt, Germany). DNaseI–AlexaFluor488 was purchased from ThermoFisher (Waltham, MA) and used at a 1:600 dilution.

Immunofluorescence staining

For immunofluorescence staining, cells were briefly rinsed with prewarmed PBS with Ca^{2+} and Mg^{2+} followed by 10 min fixation with 4% EM grade formaldehyde (Polysciences Inc., Warrington, PA). After 10 min washing with PBS, samples were permeabilized for 10 min with 0.5% Triton X-100 in PBS (Roth, Karlsruhe, Germany). Nonspecific binding was blocked by a 30 min incubation with 5% goat serum (Sigma) in PBS with 0.2% BSA (Roth, Karlsruhe, Germany) at room temperature. Following an additional washing step, cells were incubated overnight with primary antibodies diluted in PBS (1:150) plus 0.2% BSA (4°C). After 3×10 min washing with PBS, samples were incubated with secondary antibodies (1:500), and Rhodamine–phalloidin and Hoechst 33342 for 1 h, washed again 3×10 min with PBS and sealed with one drop of mounting medium.

For determination of the F-actin to G-actin ratios, cells were co-stained with phalloidin (detection of F-actin) and DNase I, which binds G-actin monomers with high affinity (Cramer et al., 2002). F-actin and G-actin levels were quantified as the value of the total phalloidin intensity/DNase I signal intensity (Nobusue et al., 2014).

Tube formation assays

Tube formation assays were performed in µ-Slides angiogenesis from ibidi (Martinsried, Germany). $11×10^3$ HUVECs were seeded onto thin layers of polymerized Matrigel™ (REF 356231, Corning Life Sciences B.V., Amsterdam, The Netherlands) and samples were incubated for the indicated time spans at 37°C under 5% CO_2.

For immunofluorescence staining of tube formation samples, cells were initially washed with PBS with Ca^{2+} and Mg^{2+} and subsequently fixed with 4% paraformaldehyde (PFA) in PBS for 40 min. Samples were permeabilized for 20 min with 0.5% Triton X-100 in and nonspecific binding was blocked by overnight incubation (4°C) with 5% goat serum in PBS supplemented with 30 µg/ml anti-mouse AffiniPure F_{ab} fragments (Jackson Immunoresearch, West Grove, PA). After 20 min washing with PBS plus 0.2% BSA, samples were incubated overnight (4°C) with primary antibodies diluted in PBS (1:150) plus 0.2% BSA. Subsequently, cells were washed three times for 20 min with PBS plus 0.2% BSA, and secondary antibodies (1:600), Hoechst 33342 and Rhodamine–phalloidin reagents were added. After overnight incubation at 4°C, samples were again washed three times for 20 min and one drop of mounting medium was added 1 h before imaging.

Retinal whole-mount staining

Wild-type C57BL/6 pups (n=4) were killed by neck dislocation at postnatal day 6 (P6) . Retina preparation and staining was performed as previously described (Pitulescu et al., 2010). In brief, eyeballs were removed and fixed for 2 h in 4% PFA in PBS. After retinal preparation, retinas were blocked and permeabilized for 2 h at room temperature with 1% BSA, 0.3% Triton X-100 in PBS. Retinal vasculature was labeled using IB4–AlexaFluor488 (ThermoFisher, Waltham, MA). Overnight incubation with primary antibodies (1:100) targeting MRTF-A and YAP was followed by several washing steps and addition of secondary antibodies (1:400). Nuclei were visualized with Hoechst 33342 and, after two more washing steps, retinas were mounted in uncoated eight-well µ-Slides using FluorSave reagent. All animal procedures were approved and controlled by the local Ethics Committee and carried out according to the guidelines of the German law for the protection of animal life.

Quantitative real-time PCR

RT-qPCR experiments were performed using an Applied Biosystems® 7300 Real-Time PCR System (ThermoFisher, Waltham, MA) with standard procedures. SYBR™ Green Master Mix (ThermoFisher) was used for cDNA amplification and detection.

The following primers were purchased from Metabion (Planegg, Germany): CTGF, forward 5'-TGGAGTTCAAGTGCCCTGAC-3', reverse 5'-CTCCCACTGCTCCTAAAGCC-3'; CYR61, forward 5'-ACCCTTCTC-CACTTGACCAG-3', reverse 5'-CTTGGCGCAGACCTTACAG-3'; GAPDH, forward 5'-ACGGGAAGCTTGTCATCAAT-3', reverse 5'-CATCGCCCCACTTGATTTT-3'; SRF, forward 5'-GTTTCAGCAGTTC-AGCTCCA-3', reverse 5'-TGTAGCTCGGTGAGGTTGCT-3'; and vinculin, forward 5'-GAGAGATATGCCACCAGCATT-3', reverse 5'-G-CACTGAGTAAGGGTCTGACTG-3'.

Transcriptomic analysis

mRNA was cleaned up from cell lysates with Sera-Mag carboxylated magnetic beads (ThermoFisher) and reverse transcribed using a slightly modified SCRB-seq protocol (Soumillon et al., 2014, preprint). During reverse transcription, sample-specific barcodes and unique molecular identifiers were incorporated into first strand cDNA. Next, samples were pooled and excess primers digested with exonuclease I (ThermoFisher).

cDNA was preamplified using KAPA HiFi HotStart polymerase (KAPA Biosystems). Sequencing libraries were constructed from cDNA using the Nextera XT Kit (Illumina, San Diego, CA). Resulting libraries were quantified and sequenced at 10 nM on a HiSeq1500 machine (Illumina, San Diego, CA). To obtain gene expression values, raw sequencing data was processed using the zUMIs pipeline (Parekh et al., 2017, preprint) using the human genome build hg19 and Ensembl gene models (GRCh37.75).

Differential expression analysis of the obtained RNA-seq read counts was carried out using edgeR, which applies generalized linear models (GLMs) based on the negative-binomial distribution while incorporating normalization factors for different library sizes (Robinson et al., 2010). Exploratory data analysis was carried out using the EnrichmentBrowser package (Geistlinger et al., 2016).

Data analysis and statistics

All images and time lapse sequences were analyzed and processed using ImageJ version 1.5. Pearson correlation coefficients were calculated using the Coloc2 plugin for ImageJ according to the available online instructions.

Statistical analysis (mean, s.d. or s.e.m., unpaired Student's t-tests, Bonferroni-Dunn-corrected multiple t-tests and Sidak-corrected one-way ANOVA tests) was performed with GraphPad Prism Version 7.0a for Mac. Unless stated otherwise, all data are derived from three independent experiments.

Acknowledgements

The authors thank Charlott Leu for the production of silicon template wafers for microcontact printing. We furthermore thank Kerstin Loske for the isolation and preparation of mouse retinas and Jana Peliskova for excellent technical assistance.

Competing interests

The authors declare no competing or financial interests.

Author contributions

Conceptualization: W.E., A.M.V., S.Z.; Methodology: F.A.G., B.J., H.W., C.Z., J.O.R.; Software: L.G.; Validation: B.J., H.W., C.Z., L.G.; Formal analysis: F.A.G.,

B.J., H.W., C.Z., W.E., L.G.; Investigation: F.A.G., C.Z.; Resources: H.W., L.G.; Data curation: C.Z., L.G.; Writing - original draft: F.A.G., S.Z.; Supervision: W.E., J.O.R., A.M.V., S.Z.; Project administration: A.M.V., S.Z.; Funding acquisition: S.Z.

Funding
This work was funded by the Deutsche Forschungsgemeinschaft (DFG) (SBF1032, projects B08 and B01).

Supplementary information
Supplementary information available online at
http://jcs.biologists.org/lookup/doi/10.1242/jcs.212886.supplemental

References

Ando, J. and Yamamoto, K. (2009). Vascular mechanobiology: endothelial cell responses to fluid shear stress. *Circ. J.* **73**, 1983-1992.
Basu S, Totty NF, Irwin MS, Sudol M, Downward J. (2003) Akt phosphorylates the Yes-associated protein, YAP, to induce interaction with 14-3-3 and attenuation of p73-mediated apoptosis. *Mol Cell.* **11**, 11–23.
Busche, S., Descot, A., Julien, S., Genth, H. and Posern, G. (2008). Epithelial cell-cell contacts regulate SRF-mediated transcription via Rac-actin-MAL signalling. *J. Cell Sci.* **121**, 1025-1035.
Buxboim, A., Irianto, J., Swift, J., Athirasala, A., Shin, J.-W., Rehfeldt, F. and Discher, D. E. (2017). Coordinated increase of nuclear tension and lamin-A with matrix stiffness outcompetes lamin-B receptor that favors soft tissue phenotypes. *Mol. Biol. Cell* **28**, 3333-3348.
Chai, J. and Tarnawski, A. S. (2002). Serum response factor: discovery, biochemistry, biological roles and implications for tissue injury healing. *J. Physiol. Pharmacol.* **53**, 147-157.
Chan, S. W., Lim, C. J., Chong, Y. F., Pobbati, A. V., Huang, C. and Hong, W. (2011). Hippo pathway-independent restriction of TAZ and YAP by angiomotin. *J. Biol. Chem.* **286**, 7018-7026.
Chatterjee, S., Fujiwara, K., Pérez, N. G., Ushio-Fukai, M. and Fisher, A. B. (2015). Mechanosignaling in the vasculature: emerging concepts in sensing, transduction and physiological responses. *Am. J. Physiol. Heart Circ. Physiol.* **308**, H1451-H1462.
Choi, H. J., Zhang, H., Park, H., Choi, K.-S., Lee, H. W., Agrawal, V., Kim, Y. M. and Kwon, Y. G. (2015). Yes-associated protein regulates endothelial cell contact-mediated expression of angiopoietin-2. *Nat. Commun.* **6**, 6943.
Corada, M., Liao, F., Lindgren, M., Lampugnani, M. G., Breviario, F., Frank, R., Muller, W. A., Hicklin, D. J., Bohlen, P. and Dejana, E. (2001). Monoclonal antibodies directed to different regions of vascular endothelial cadherin extracellular domain affect adhesion and clustering of the protein and modulate endothelial permeability. *Blood* **97**, 1679-1684.
Cramer, L. P., Briggs, L. J. and Dawe, H. R. (2002). Use of fluorescently labelled deoxyribonuclease I to spatially measure G-actin levels in migrating and non-migrating cells. *Cell Motil. Cytoskeleton* **51**, 27-38.
Cui, Y., Hameed, F. M., Yang, B., Lee, K., Pan, C. Q., Park, S. and Sheetz, M. (2015). Cyclic stretching of soft substrates induces spreading and growth. *Nat. Commun.* **6**, 6333.
Dechat, T., Pfleghaar, K., Sengupta, K., Shimi, T., Shumaker, D. K., Solimando, L. and Goldman, R. D. (2008). Nuclear lamins: major factors in the structural organization and function of the nucleus and chromatin. *Genes Dev.* **22**, 832-853.
Dupont, S. (2015). Role of YAP/TAZ in cell-matrix adhesion-mediated signalling and mechanotransduction. *Exp. Cell Res.* **343**, 42-53.
Dupont, S., Morsut, L., Aragona, M., Enzo, E., Giulitti, S., Cordenonsi, M., Zanconato, F., Le Digabel, J., Forcato, M., Bicciato, S. et al. (2011). Role of YAP/TAZ in mechanotransduction. *Nature* **474**, 179-183.
Eliceiri, B. P. and Cheresh, D. A. (2001). Adhesion events in angiogenesis. *Curr. Opin. Cell Biol.* **13**, 563-568.
Elosegui-Artola, A., Andreu, I., Beedle, A. E. M., Lezamiz, A., Uroz, M., Kosmalska, A. J., Oria, R., Kechagia, J. Z., Rico-Lastres, P., Le Roux, A. L. et al. (2017). Force triggers YAP nuclear entry by regulating transport across nuclear pores. *Cell* **171**, 1397-1410.e14.
Esnault, C., Stewart, A., Gualdrini, F., East, P., Horswell, S., Matthews, N. and Treisman, R. (2014). Rho-actin signaling to the MRTF coactivators dominates the immediate transcriptional response to serum in fibroblasts. *Genes Dev.* **28**, 943-958.
Franco, C. A., Mericskay, M., Parlakian, A., Gary-Bobo, G., Gao-Li, J., Paulin, D., Gustafsson, E. and Li, Z. (2008). Serum response factor is required for sprouting angiogenesis and vascular integrity. *Dev. Cell* **15**, 448-461.
Franco, C. A., Blanc, J., Parlakian, A., Blanco, R., Aspalter, I. M., Kazakova, N., Diguet, N., Mylonas, E., Gao-Li, J., Vaahtokari, A. et al. (2013). SRF selectively controls tip cell invasive behavior in angiogenesis. *Development* **140**, 2321-2333.
Gaspar, P. and Tapon, N. (2014). Sensing the local environment: actin architecture and Hippo signalling. *Curr. Opin. Cell Biol.* **31**, 74-83.
Geistlinger, L., Csaba, G. and Zimmer, R. (2016). Bioconductor's EnrichmentBrowser: seamless navigation through combined results of set- & network-based enrichment analysis. *BMC Bioinformatics* **17**, 45.
Giampietro, C., Disanza, A., Bravi, L., Barrios-Rodiles, M., Corada, M., Frittoli, E., Savorani, C., Lampugnani, M. G., Boggetti, B., Niessen, C. et al. (2015). The actin-binding protein EPS8 binds VE-cadherin and modulates YAP localization and signaling. *J. Cell Biol.* **211**, 1177-1192.
Hermann, M. R., Jakobson, M., Colo, G. P., Rognoni, E., Jakobson, M., Kupatt, C., Posern, G. and Fassler, R. (2016). Integrins synergize to induce expression of the MRTF-A/SRF target gene ISG15 for promoting cancer cell invasion. *J. Cell Sci.* **129**, 1391-1403.
Hinkel, R., Trenkwalder, T., Petersen, B., Husada, W., Gesenhues, F., Lee, S., Hannappel, E., Bock-Marquette, I., Theisen, D., Leitner, L. et al. (2014). MRTF-A controls vessel growth and maturation by increasing the expression of CCN1 and CCN2. *Nat. Commun.* **5**, 3970.
Ireland, G. W., Dopping-Hepenstal, P., Jordan, P. and O'neill, C. (1987). Effect of patterned surfaces of adhesive islands on the shape, cytoskeleton, adhesion and behaviour of Swiss mouse 3T3 fibroblasts. *J. Cell Sci. Suppl.* **8**, 19-33.
Isermann, P. and Lammerding, J. (2013). Nuclear mechanics and mechanotransduction in health and disease. *Curr. Biol.* **23**, R1113-R1121.
Kim, D. H., Cho, S. and Wirtz, D. (2014). Tight coupling between nucleus and cell migration through the perinuclear actin cap. *J. Cell Sci.* **127**, 2528-2541.
Kim, T., Hwang, D., Lee, D., Kim, J. H., Kim, S. Y. and Lim, D. S. (2016). MRTF potentiates TEAD-YAP transcriptional activity causing metastasis. *EMBO J.* **36**, 520-535.
Mammoto, A., Mammoto, T. and Ingber, D. E. (2012). Mechanosensitive mechanisms in transcriptional regulation. *J. Cell Sci.* **125**, 3061-3073.
Mana-Capelli, S., Paramasivam, M., Dutta, S. and Mccollum, D. (2014). Angiomotins link F-actin architecture to Hippo pathway signaling. *Mol. Biol. Cell* **25**, 1676-1685.
Marti, P., Stein, C., Blumer, T., Abraham, Y., Dill, M. T., Pikiolek, M., Orsini, V., Jurisic, G., Megel, P., Makowska, Z. et al. (2015). YAP promotes proliferation, chemoresistance, and angiogenesis in human cholangiocarcinoma through TEAD transcription factors. *Hepatology* **62**, 1497-1510.
Mateus, R., Lourenco, R., Fang, Y., Brito, G., Farinho, A., Valerio, F. and Jacinto, A. (2015). Control of tissue growth by Yap relies on cell density and F-actin in zebrafish fin regeneration. *Development* **142**, 2752-2763.
Mendez, M. G. and Janmey, P. A. (2012). Transcription factor regulation by mechanical stress. *Int. J. Biochem. Cell Biol.* **44**, 728-732.
Miralles, F., Posern, G., Zaromytidou, A. I. and Treisman, R. (2003). Actin dynamics control SRF activity by regulation of its coactivator MAL. *Cell* **113**, 329-342.
Mokalled, M. H., Carroll, K. J., Cenik, B. K., Chen, B., Liu, N., Olson, E. N. and Bassel-Duby, R. (2015). Myocardin-related transcription factors are required for cardiac development and function. *Dev. Biol.* **406**, 109-116.
Nakajima, H., Yamamoto, K., Agarwala, S., Terai, K., Fukui, H., Fukuhara, S., Ando, K., Miyazaki, T., Yokota, Y., Schmelzer, E. et al. (2017). Flow-dependent endothelial YAP regulation contributes to vessel maintenance. *Dev. Cell* **40**, 523-536 e6.
Nobusue, H., Onishi, N., Shimizu, T., Sugihara, E., Oki, Y., Sumikawa, Y., Chiyoda, T., Akashi, K., Saya, H. and Kano, K. (2014). Regulation of MKL1 via actin cytoskeleton dynamics drives adipocyte differentiation. *Nat. Commun.* **5**, 3368.
O'connor, J. W. and Gomez, E. W. (2013). Cell adhesion and shape regulate TGF-beta1-induced epithelial-myofibroblast transition via MRTF-A signaling. *PLoS ONE* **8**, e83188.
O'connor, J. W., Mistry, K., Detweiler, D., Wang, C. and Gomez, E. W. (2016). Cell-cell contact and matrix adhesion promote alphaSMA expression during TGFbeta1-induced epithelial-myofibroblast transition via Notch and MRTF-A. *Sci. Rep.* **6**, 26226.
O'neill, C., Jordan, P. and Ireland, G. (1986). Evidence for two distinct mechanisms of anchorage stimulation in freshly explanted and 3T3 Swiss mouse fibroblasts. *Cell* **44**, 489-496.
Pan, D. (2010). The hippo signaling pathway in development and cancer. *Dev. Cell* **19**, 491-505.
Parekh, S., Ziegenhain, C., Vieth, B., Enard, W. and Hellmann, I. (2017). zUMIs: A fast and flexible pipeline to process RNA sequencing data with UMIs. *bioRxiv*. 153940. doi:10.1101/153940
Pitulescu, M. E., Schmidt, I., Benedito, R. and Adams, R. H. (2010). Inducible gene targeting in the neonatal vasculature and analysis of retinal angiogenesis in mice. *Nat. Protoc.* **5**, 1518-1534.
Plessner, M., Melak, M., Chinchilla, P., Baarlink, C. and Grosse, R. (2015). Nuclear F-actin formation and reorganization upon cell spreading. *J. Biol. Chem.* **290**, 11209-11216.
Posern, G. and Treisman, R. (2006). Actin' together: serum response factor, its cofactors and the link to signal transduction. *Trends Cell Biol.* **16**, 588-596.
Posern, G., Sotiropoulos, A. and Treisman, R. (2002). Mutant actins demonstrate a role for unpolymerized actin in control of transcription by serum response factor. *Mol. Biol. Cell* **13**, 4167-4178.
Potente, M., Gerhardt, H. and Carmeliet, P. (2011). Basic and therapeutic aspects of angiogenesis. *Cell* **146**, 873-887.

Robinson, M. D., Mccarthy, D. J. and Smyth, G. K. (2010). edgeR: a Bioconductor package for differential expression analysis of digital gene expression data. *Bioinformatics* **26**, 139-140.
Santos-Oliveira, P., Correia, A., Rodrigues, T., Ribeiro-Rodrigues, T. M., Matafome, P., Rodriguez-Manzaneque, J. C., Seica, R., Girao, H. and Travasso, R. D. (2015). The Force at the Tip - Modelling Tension and Proliferation in Sprouting Angiogenesis. *PLoS Comput. Biol.* **11**, e1004436.
Schuster, S. L., Segerer, F. J., Gegenfurtner, F. A., Kick, K., Schreiber, C., Albert, M., Vollmar, A. M., Radler, J. O. and Zahler, S. (2016). Contractility as a global regulator of cellular morphology, velocity, and directionality in low-adhesive fibrillary micro-environments. *Biomaterials* **102**, 137-147.
Seifert, A. and Posern, G. (2017). Tightly controlled MRTF-A activity regulates epithelial differentiation during formation of mammary acini. *Breast Cancer Res.* **19**, 68.
Simon, D. N. and Wilson, K. L. (2011). The nucleoskeleton as a genome-associated dynamic 'network of networks'. *Nat. Rev. Mol. Cell Biol.* **12**, 695-708.
Soumillon, M., Cacchiarelli, D., Semrau, S., Van Oudenaarden, A. and Mikkelsen, T. S. (2014). Characterization of directed differentiation by high-throughput single-cell RNA-Seq. *bioRxiv* 003236.
Speight, P., Kofler, M., Szaszi, K. and Kapus, A. (2016). Context-dependent switch in chemo/mechanotransduction via multilevel crosstalk among cytoskeleton-regulated MRTF and TAZ and TGFbeta-regulated Smad3. *Nat. Commun.* **7**, 11642.
Stiles, J. M., Pham, R., Rowntree, R. K., Amaya, C., Battiste, J., Boucheron, L. E., Mitchell, D. C. and Bryan, B. A. (2013). Morphological restriction of human coronary artery endothelial cells substantially impacts global gene expression patterns. *FEBS J.* **280**, 4474-4494.
Thomas, C. H., Collier, J. H., Sfeir, C. S. and Healy, K. E. (2002). Engineering gene expression and protein synthesis by modulation of nuclear shape. *Proc. Natl. Acad. Sci. USA* **99**, 1972-1977.
Tzima, E., Irani-Tehrani, M., Kiosses, W. B., Dejana, E., Schultz, D. A., Engelhardt, B., Cao, G., Delisser, H. and Schwartz, M. A. (2005). A mechanosensory complex that mediates the endothelial cell response to fluid shear stress. *Nature* **437**, 426-431.
Versaevel, M., Braquenier, J. B., Riaz, M., Grevesse, T., Lantoine, J. and Gabriele, S. (2014). Super-resolution microscopy reveals LINC complex recruitment at nuclear indentation sites. *Sci. Rep.* **4**, 7362.
Wang, K.-C., Yeh, Y.-T., Nguyen, P., Limqueco, E., Lopez, J., Thorossian, S., Guan, K.-L., Li, Y.-J. and Chien, S. (2016). Flow-dependent YAP/TAZ activities regulate endothelial phenotypes and atherosclerosis. *Proc. Natl. Acad. Sci. USA* **113**, 11525-11530.
Xu, S., Koroleva, M., Yin, M. and Jin, Z. G. (2016). Atheroprotective laminar flow inhibits Hippo pathway effector YAP in endothelial cells. *Transl. Res.* **176**, 18-28 e2.
Yu, F. X. and Guan, K. L. (2013). The Hippo pathway: regulators and regulations. *Genes Dev.* **27**, 355-371.
Yu, O. M., Miyamoto, S. and Brown, J. H. (2015). Myocardin-related transcription factor A and yes-associated protein exert dual control in G protein-coupled receptor- and RhoA-mediated transcriptional regulation and cell proliferation. *Mol. Cell. Biol.* **36**, 39-49.
Zanconato, F., Forcato, M., Battilana, G., Azzolin, L., Quaranta, E., Bodega, B., Rosato, A., Bicciato, S., Cordenonsi, M. and Piccolo, S. (2015). Genome-wide association between YAP/TAZ/TEAD and AP-1 at enhancers drives oncogenic growth. *Nat. Cell Biol.* **17**, 1218-1227.
Zhao, B., Wei, X., Li, W., Udan, R. S., Yang, Q., Kim, J., Xie, J., Ikenoue, T., Yu, J., Li, L. et al. (2007). Inactivation of YAP oncoprotein by the Hippo pathway is involved in cell contact inhibition and tissue growth control. *Genes Dev.* **21**, 2747-2761.
Zhao, B., Li, L., Lei, Q. and Guan, K. L. (2010). The Hippo-YAP pathway in organ size control and tumorigenesis: an updated version. *Genes Dev.* **24**, 862-874.
Zhao, B., Li, L., Wang, L., Wang, C. Y., Yu, J. and Guan, K. L. (2012). Cell detachment activates the Hippo pathway via cytoskeleton reorganization to induce anoikis. *Genes Dev.* **26**, 54-68.